Check for updates

Dilution of contact frequency between superenhancers by loop extrusion at interfaces†‡

Tetsuya Yamamoto [*ab] and Helmut Schiessel[c]

The loop extrusion theory predicts that cohesin acts as a molecular motor that extrudes chromatin fibers to produce loops. Hi-C experiments have detected relatively high contact frequencies between superenhancers. These probably result from the fact that superenhancers are localized at condensates of transcriptional activators and coactivators. The contact frequency between superenhancers is enhanced by auxin treatment that removes cohesin from chromatin. Motivated by these experimental results, we here treat chromatin at the surface of a condensate as a loop extruding polymer brush. Our theory predicts that the lateral pressure generated by the brush decreases with decreasing the loading rate of cohesin. This is because loop extrusion actively transfers chain segments at the vicinity of the interface. Our theory thus predicts that the increase of contact frequency by auxin treatment results from the fact that suppressing the loop extrusion process induces the dissolution of molecular components to the nucleoplasm, decreasing the average distance between superenhancers.

1 Introduction

In eukaryotic cells, DNA is packed into a nucleus by forming a complex, called chromatin, with histone proteins. On much larger scales, chromatin is composed of topologically associated domains (TADs), contiguous regions of enriched contact frequency that are isolated from other regions.[1,2] In 40% of TADs, the contact frequency between the two ends is much larger than between other pairs, implying that these TADs are composed of loops of chromatin.[3] The loop extrusion theory predicts that cohesin, a ring-shaped protein complex, acts as a molecular motor and extrudes the chromatin fiber to produce a loop until it collides with another protein factor, called CTCF, which is localized at the ends of each TAD.[4,5] Whether cohesin acts as a molecular motor or operates *via* other mechanisms[6–8] remains to be elucidated. However, this theory predicts features that agree well with those deduced from experimental contact frequency maps.

Auxin-induced degron techniques allow to remove cohesin from chromatin in response to the dosing of auxin.§[9] Removing cohesin

from chromatin by using the auxin treatment eliminates the chromatin loops.[10] Remaining contacts are between superenhancers, clusters of enhancers¶ that are occupied by a high density of transcription machinery. Indeed, the contacts between superenhancers become more frequent by auxin treatment. This treatment decreases the transcription rate of genes that are activated by superenhancers by more than twofold (as measured by PRO-seq technique‖, 6 hours after the cohesin removal), while it does not change the transcription rate of other genes significantly.[10] Elucidating the nature of the contacts between superenhancers, the structure of chromatin assembled by those contacts, and the influence of loop extrusion on the structure are important steps to understand the physics behind transcription regulation by loop extrusion.

Transcriptional activators and coactivators form liquid condensates of micrometer size in the nucleus of a living cell, probably by phase separation or microphase separation, and superenhancers are localized at these condensates.[11,12] The frequent contacts between superenhancers, as detected by Hi-C experiments,[10] imply that multiple superenhancers (or multiple enhancers separated by a long genomic distance) are localized at the condensates. The superenhancers probably attach to the surface of the condensate *via* transcriptional activators due to the fact that activators are localized inside the condensates and chromatin is repelled from the condensates.[13,14] The resulting structure may be analogous to a microemulsion, here stabilized

[a] *Department of Materials Physics, Nagoya University, Furo-cho, Chikusa-ku, Nagoya, Japan. E-mail: tyamamoto@nuap.nagoya-u.ac.jp; Tel: +81-52-788-6076*

[b] *PRESTO, Japan Science and Technology Agency (JST) – 4-1-8 Honcho, Kawaguchi, Saitama, 332-0012, Japan*

[c] *Instituut-Lorentz for Theoretical Physics, Leiden University – Niels Bohrweg 2, Leiden, 2333 CA, The Netherlands*

† The Mathematica notebook file (loopingbrushver10.nb) used to derive the data that support the findings of this study is available in figshare with identifier (https://doi.org/10.6084/m9.figshare.9750947).

‡ Electronic supplementary information (ESI) available. See DOI: 10.1039/c9sm01454c

§ With this technique, dosed auxin activates the ubiquitin ligase that drives the degradation of tagged proteins.

¶ Enhancers are DNA sequences that activate transcription by binding to promoters, from which RNA polymerase starts transcription.

‖ PRO-seq is a technique to detect actively transcribed genes by mapping RNA polymerase II, an enzyme that synthesizes messenger RNA.

by chromatin.[14,15] With this analogy, the stability and size of the condensates are determined by the lateral pressure generated by the chromatin at the interface. The lateral pressure generated by the chromatin complex may be modulated by the loop extrusion process and this may account for the fact that the contact frequency between superenhancers increases by removing cohesin from chromatin. The objective of this paper is to demonstrate this concept by using a simple model, rather than to build a detailed model of chromatin.

We here treat chromatin at the interface as a loop extruding polymer brush to calculate the generated lateral pressure. We predict that this pressure increases with increasing cohesin loading rate and/or increasing rate of loop extrusion. This is because the loop extrusion process increases the local concentration of chromatin chain segments and this increases the repulsive interactions between them. This prediction implies that the size of the condensate increases *via* Ostwald ripening and thus the contact frequency between superenhancers decreases due to the loop extrusion process.

2 Model

We treat chromatin at the interface between a condensate and the solution as a polymer brush whose structure is actively modified through the action of loop extrusion. The chromatin fibers are end-grafted to the interface with grafting density σ *via* enhancers at their ends. Chromatin brush models have been used before as simplified models for chromatin grafted at interfaces.[16,17] The chromatin fibers are longer than the Kuhn length and are in a solution at physiological salt concentration. We thus treat each chromatin fiber as an electrically neutral flexible chain that is composed of N Kuhn segments, each of length l_a. We use the Alexander approximation that assumes that the concentration of the segments is uniform in the brush.[18,19] Experiments suggest that the loops at the vicinity of superenhancers are recovered relatively fast when auxin is washed out, implying that there is a loading site at the vicinity of superenhancers.[10] We thus treat the case in which cohesin is loaded on the grafted end of the chain with average loading rate τ_{on}^{-1} and extrudes segments with a constant rate τ_s^{-1}. The average time of the loop extrusion process thus has the form

$$\tau_{ex} = N\tau_s. \qquad (1)$$

The cohesin molecule divides the chain into a loop and an arm subchain; the segments of the loop subchain are already extruded whereas the segments of the arm subchain have not yet been extruded, see Fig. 1. In general, cohesin is unloaded from chromatin with a constant rate anywhere in the region between two CTCF proteins (of converging orientation). For simplicity, we here treat the case in which cohesin is unloaded only when it reaches the free end of the chain. We use this model to predict the average osmotic pressure generated by loop extrusion as a function of the average cohesin loading rate τ_{on}^{-1}, of the average time τ_{ex} per loop extrusion process, and of the chain relaxation time τ_N. For simplicity, we treat only the
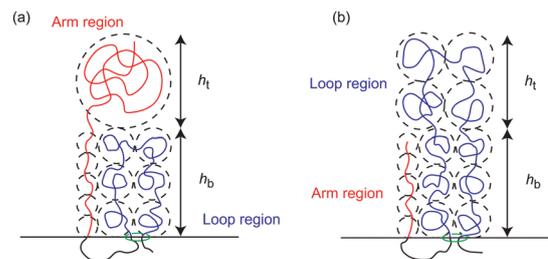

Fig. 1 Chromatin at an interface between a condensate (of transcription activators and coactivators) and the exterior solution is modeled as a polymer brush. Cohesin molecules (green circle) are loaded on the chain from the grafting end and extrude segments from the arm region (shown in red) to the loop region (shown in blue). In the beginning the height of the arm region is larger than the height of the loop region (a). For longer time scales, the height of the loop region becomes larger than the height of the arm region (b).

case where the average loading time τ_{on} is larger than the average time τ_{ex} per loop extrusion event, *i.e.* where each polymer carries at most one cohesin molecule.

For simplicity, we use Onsager's variational principle[20] to derive the time evolution equation of the brush height. Onsager's principle states that the time development of a dissipative system is determined by the minimization of the Rayleighan

$$\mathcal{R} = \Phi + \dot{F}, \qquad (2)$$

where Φ is the dissipation function and F is the free energy (here and in the following $\dot{f}(t)$ denotes the time derivative of function $f(t)$). The brush is composed of a bottom layer, in which the loop and arm subchains coexist, and a top layer, in which only one of the subchains exists, see Fig. 1. The height of the top layer is denoted by h_t and the height of the bottom layer by h_b. The dynamics of the brush is represented by the dynamics of the position of the brush top, $z_t(t) = h (\equiv h_t + h_b)$, and the position of the interface between the two layers, $z_b(t) = h_b$. The dissipation function Φ per chain has the form

$$\Phi = \frac{1}{2}\zeta N_t \dot{h}^2 + \frac{1}{2}\zeta N \dot{h_b}^2. \qquad (3)$$

The first term of eqn (3) is the energy dissipation due to the motion of the brush top (while the position of the interface is fixed) and the second term of eqn (3) is the energy dissipation due to the motion of the layer interface (while the position of the brush top is fixed). Eqn (3) treats the case in which the concentration of the chain segments in the brush region is large enough to screen the hydrodynamic interactions between chain segments so that the friction constant is proportional to the number of the segments in motion. N_t is the number of Kuhn segments in the top layer. Only the segments in the top layer move when the position of the brush top moves while the position of the layer interface is fixed. In contrast, the segments of both layers move when the position of the layer interface moves while the position of the brush top is fixed.

The free energy of the brush (per chain) has the form

$$F = F_{lp} + F_{arm} + \Pi_b(2A_{lp} + A_b) + \Pi_t A_t - \mu(N_{lp} + N_b + N_t - N), \qquad (4)$$

where F_{lp} is the free energy of the subchain in the loop region and F_{arm} is the free energy of the subchain in the arm region. The subscripts 'lp' and 'arm' stand for the loop and arm regions, respectively. The lateral osmotic pressure, Π_b and Π_t, and the chemical potential μ are Lagrange multipliers that ensure that the area per chain and the number of segments are constant. The subscripts 'b' and 't' stand for the bottom and top layers, respectively. A_{lp} is the area occupied by one of the two subchains composing a loop (for simplicity, we treat the loop as two subchains connected at the top), see the blue subchain in Fig. 1, and A_b is the area occupied by the subchain of the arm region in the bottom layer, see the red chain in Fig. 1. A_t $(= \sigma^{-1})$ is the area per chain. N_{lp} is the number of Kuhn segments in the loop region and N_b is the number of Kuhn segments of the arm subchain in the bottom layer.

We here analyze the dynamics of the chains after a cohesin molecule is loaded onto a chain at $t = 0$. We start with the dynamics on short time scales, $t < t_{th}$, when the space in the top layer is occupied by part of the arm subchain, see Fig. 1(a). The free energy contributions F_{lp} and F_{arm} have then the forms

$$\frac{F_{lp}}{k_B T} = \frac{3}{2} \frac{4 h_b^2}{N_{lp} l_a^2} + v \frac{\sigma_{lp} N_{lp}^2}{2 h_b} \quad (5)$$

$$\frac{F_{arm}}{k_B T} = \frac{3}{2} \frac{h_b^2}{N_b l_a^2} + v \frac{\sigma_b N_b^2}{h_b} + \frac{3}{2} \frac{h_t^2}{N_t l_a^2} + v \frac{\sigma N_t^2}{h_t}. \quad (6)$$

The derivation of eqn (5) and (6) by using blob arguments is shown in Section S1.1 of the ESI.‡ The first term of eqn (5) is the free energy due to the entropic elasticity of the loop region and the second term is the free energy due to the excluded volume interactions between the segments in the loop region. The number N_{lp} of segments in the loop region has the form $N_{lp} = t/\tau_s$ for this time scale, see Fig. 1. v is the second virial coefficient that accounts for the excluded volume interactions between chain segments. The loop region is composed of two subchains of length $N_{lp}/2$ which is accounted for by the numerical factors in eqn (5). σ_{lp} $(= 1/A_{lp})$ is the number of loop subchains per unit area. Furthermore, N_t segments of the arm region occupy the top layer above the loop region and N_b segments are in the bottom layer. The first and third terms of eqn (6) are the free energy contributions due to the entropic elasticity of the arm region in the bottom and top layers, respectively. The corresponding free energy contributions due to the excluded volume interactions are given by the second and fourth terms. σ_b $(= 1/A_b)$ is the number of arm chains in the bottom layer per unit area. This approach takes into account the longest relaxation mode due to the entropic elasticity of the chain and the relaxation process by the excluded volume interactions.

The lateral osmotic pressures in the top and bottom layers are given by

$$\frac{\Pi_t}{k_B T} = v \frac{\sigma^2 N_t^2}{h_t} \quad (7)$$

$$\frac{\Pi_b}{k_B T} = v \frac{\sigma_{lp}^2 N_{lp}^2}{4 h_b} = v \frac{\sigma_b^2 N_b^2}{h_b}, \quad (8)$$

which follow from minimizing the free energy, eqn (4), with respect to the areas (per chain) A_t, A_{lp}, and A_b. Minimizing the free energy with respect to the segment numbers N_t and N_b, leads to

$$\frac{\mu}{k_B T} = -\frac{3}{2} \frac{h_b^2}{N_b^2 l_a^2} + 2 v \frac{N_b \sigma_{lp}}{h_b} = -\frac{3}{2} \frac{h_t^2}{N_t^2 l_a^2} + 2 v \frac{\sigma N_t}{h_t}. \quad (9)$$

With eqn (8) and (9), we assume that the relaxation in the lateral direction and the transfer of segments between the top and bottom layers are relatively fast. The number densities σ_b and σ_{lp} are given by

$$\sigma_{lp} = \frac{2 \sigma (N_b + N_{lp})}{N_{lp}} \quad (10)$$

$$\sigma_b = \frac{\sigma (N_b + N_{lp})}{N_b}. \quad (11)$$

These equations are derived by using eqn (8) and the relationship $\sigma^{-1} = 2 \sigma_{lp}^{-1} + \sigma_b^{-1}$. We assume that the grafting density is constant throughout the loop extrusion and relaxation processes (see also Discussion).

Minimizing the Rayleighan, eqn (2), with respect to $\dot{h}$ and $\dot{h}_{lp}$ leads to the time evolution equations of brush heights

$$\frac{d}{dt} h(t) = \frac{k_B T}{N_t \zeta} \left(-\frac{3 h_t(t)}{N_t l_a^2} + v \frac{\sigma N_t^2}{h_t^2(t)} \right) \quad (12)$$

$$\frac{d}{dt} h_b(t)$$
$$= \frac{k_B T}{N \zeta} \left(-\frac{12 h_b(t)}{N_{lp} l_a^2} - \frac{3 h_b(t)}{N_b l_a^2} + v \frac{\sigma (N_{lp} + N_b)^2}{h_b^2(t)} + \frac{3 h_t(t)}{N_t l_a^2} - v \frac{\sigma N_t^2}{h_t^2(t)} \right), \quad (13)$$

where we made use of the relationships (10) and (11). Eqn (9), (12), and (13) and the relationship $N_t = N - N_b - t/\tau_s$ lead to equations for the segment number $N_b(t)$ and the heights, $h(t)$ and $h_b(t)$. The lateral osmotic pressure $\Pi_\parallel = \Pi_t + \Pi_b$ is derived by substituting $N_b(t)$, $h(t)$, and $h_b(t)$ into eqn (7) and (8).

For longer time scales, $t_{th} < t < \tau_{ex}$, the space in the top layer is occupied by part of the loop subchain, see Fig. 1(b). The free energy contributions F_{lp} and F_t are then given by

$$\frac{F_{lp}}{k_B T} = \frac{3}{2} \frac{4 h_b^2}{N_{lp} l_a^2} + v \frac{\sigma_{lp} N_{lp}^2}{2 h_b} + \frac{3}{2} \frac{4 h_t^2}{N_t l_a^2} + v \frac{\sigma N_t^2}{h_t} \quad (14)$$

$$\frac{F_{arm}}{k_B T} = \frac{3}{2} \frac{h_b^2}{N_b l_a^2} + v \frac{\sigma_b N_b^2}{2 h_b}. \quad (15)$$

The derivation of eqn (14) and (15) via blob arguments is shown in Section S1.2 in the ESI.‡ The first and third terms of eqn (14) are the free energy contributions due to the entropic elasticity of the loop subchain in the bottom and top layers, respectively. The second and third terms are the corresponding terms describing the excluded volume interactions. The first term of eqn (15) is the free energy due to the entropic elasticity of the

arm subchain and the second term represents the free energy contribution from the excluded volume interactions between segments of the arm subchain.

Minimizing the free energy, eqn (4), with respect to the segment numbers N_b and N_t, we obtain

$$\frac{\mu}{k_B T} = -\frac{6h_b^2}{N_{lp}^2 l_a^2} + \frac{\sigma_{lp} N_{lp}}{h_b} = -\frac{6h_t^2}{N_t^2 l_a^2} + v\frac{2\sigma N_t}{h_t}. \qquad (16)$$

Minimizing the free energy with respect to the areas A_t, A_b, and A_{lp}, leads to the lateral osmotic pressure, Π_t and Π_b, in the same form as eqn (7) and (8). The time evolution equations for the heights h and h_b have the form

$$\frac{d}{dt}h(t) = \frac{k_B T}{\zeta N_t}\left(-\frac{12h_t(t)}{N_t l_a^2} + v\frac{\sigma N_t^2}{h_t^2(t)}\right) \qquad (17)$$

$$\frac{d}{dt}h_b(t)$$
$$= \frac{k_B T}{\zeta N}\left(-\frac{3h_b(t)}{N_b l_a^2} - \frac{12h_b(t)}{N_{lp} l_a^2} + v\frac{\sigma(N_{lp}+N_b)^2}{h_b^2(t)} + \frac{12h_t(t)}{N_t l_a^2} - v\frac{\sigma N_t^2}{h_t^2(t)}\right) \qquad (18)$$

which follow from minimizing the Rayleighan, eqn (2), with respect to $\dot{h}$ and $\dot{h}_{lp}$. Eqn (16), (17), and (18) and the relationship, $N_t = t/\tau_s - N_{lp}$, lead to equations for the segment number N_{lp} and the heights h and h_b. The lateral osmotic pressure, $\Pi_\parallel = \Pi_t + \Pi_b$, is derived by substituting these forms into eqn (7) and (8).

The cohesin molecule is unloaded from the chromatin fiber at $t = \tau_{ex}$. The chain relaxes until another cohesin is loaded at $t = \tau_{on}$. During the relaxation process, $\tau_{ex} < t < \tau_{on}$, the dissipation function Φ and the free energy F have the form

$$\Phi = \frac{1}{2}\zeta N\dot{h}^2 \qquad (19)$$

$$\frac{F}{k_B T} = \frac{3}{2}\frac{h^2}{N l_a^2} + v\frac{\sigma N^2}{h}. \qquad (20)$$

Minimizing the Rayleighan leads to the form

$$\frac{d}{dt}h(t) = \frac{k_B T}{\zeta N}\left(-\frac{3h(t)}{N l_a^2} + v\frac{\sigma N^2}{h^2(t)}\right). \qquad (21)$$

The lateral osmotic pressure is derived by substituting the solution of eqn (21) into

$$\frac{\Pi_\parallel}{k_B T} = v\frac{\sigma^2 N^2}{h}. \qquad (22)$$

In the limit of large average loading time $(\tau_{on} \to \infty)$, our theory returns to the Alexander model of a polymer brush. The Alexander model predicts that the brush height and the lateral pressure of a polymer brush at thermodynamic equilibrium are given by

$$h_{Alx} = N l_a\left(\frac{\sigma v}{3 l_a}\right)^{1/3} \qquad (23)$$

$$\frac{\Pi_{Alx}}{k_B T} = v\frac{\sigma^2 N^2}{h_{Alx}}. \qquad (24)$$

When the excluded volume interactions between chain segments are negligible $(v \to 0)$, our theory predicts that the longest relaxation time of the chain is the Rouse time

$$\tau_N = \frac{\zeta l_a^2 N^2}{3 k_B T}. \qquad (25)$$

3 Results

Our theory predicts that the dynamics of the brush height depends on two ratios of time scales

$$\alpha = \frac{\tau_{ex}}{\tau_N}, \qquad (26)$$

and τ_{on}/τ_N, see also eqn (1) and (25).

We first treat the simple case in which the average cohesin loading time τ_{on} is larger than the longest relaxation time τ_N. Therefore, when a cohesin molecule is loaded onto a chain, that chain is typically completely relaxed with a height given by the equilibrium value h_{Alx}, eqn (23). Because the chain is extruded at a constant rate, the height of the loop increases approximately linearly with time, see Fig. 2. The linear dependence of the height of the loop on the short time scale results from the fact that the dynamics of the loop is governed by the excluded volume interactions. For $t < t_{th}$, the height of the loop subchain $h_{lp}(t)$ $(= h_b)$ has the asymptotic form

$$\frac{h_{lp}(t)}{h_{Alx}} = \alpha^{1/3}\frac{t}{\tau_{ex}}. \qquad (27)$$
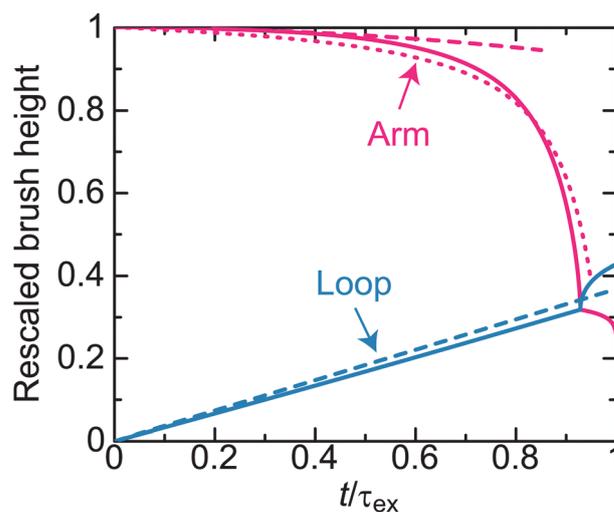

Fig. 2 The height (rescaled by the height h_{Alx} of the Alexander brush) of the arm (magenta) and the loop (cyan) is shown as a function of time t (rescaled by the time scale τ_{ex} of the loop extrusion process). The time scale ratio α (= τ_{ex}/τ_N) is fixed to 0.05. Calculations were performed by assuming that the grafting density σ is constant. The solid curves are derived by numerically calculating eqn (9), (12) and (13) in the short time regime and eqn (16), (17) and (18) in the long time regime. The cyan broken curve is the asymptotic form of the height of the loop subchains for the short time regime, see eqn (27). The magenta broken curve is the asymptotic form of the arm subchain for the short time regime, see eqn (28), and the magenta dotted curve is an approximate form for this time regime, see eqn (29).

for small time scale ratio α, see the broken cyan curve in Fig. 2. The derivation of eqn (27) is shown *via* two different ways in S3 and S4 of the ESI.‡

The height of the arm subchain does not change for a period of time although chain segments are constantly transferred from the arm region to the loop region. Recently we have used an extension of the Rouse model to predict that the conformation of the chain does not respond to the loop extrusion process before the tension generated by this process has travelled from the extruded segment to the free end.[15] The present model does not treat local segment motion and thus tension propagation is taken into account only implicitly for the longest chain relaxation time τ_N. However, it still accounts for the delayed response of the brush height to loop extrusion and the excluded volume interactions through a Flory-type free energy. With this model, the height $h_{arm}(t)$ of the arm subchain has the asymptotic form

$$\frac{h_{arm}(t)}{h_{Alx}} = \tilde{h}_0 + \alpha \frac{1 - \tilde{h}_0^3}{\tilde{h}_0^2} \frac{t}{\tau_{ex}} - \alpha \frac{1 + 2\tilde{h}_0^3}{2\tilde{h}_0^2} \left(\frac{t}{\tau_{ex}}\right)^2 \qquad (28)$$

for $t \to 0$ and small values of α, where $\tilde{h}_0$ ($= h_0/h_{Alx}$) is the brush height h_0 at $t = 0$, rescaled by the equilibrium brush height h_{Alx}, see broken magenta curve in Fig. 2. The derivation of eqn (28) is provided in S3 of the ESI.‡ Eqn (28) is effective only for very short time. Neglecting the excluded volume interactions (except for the fact that we use eqn (27) for the height $h_{lp}(t)$ of the loop subchain) leads to an approximate form

$$h_{arm}(t) = h_0 e^{-\alpha t/(\tau_{ex} - t)}, \qquad (29)$$

for small time ratio α, see the dotted magenta curve in Fig. 2. The derivation of eqn (29) is presented in S4 of the ESI.‡

For later times the height of the arm subchain decreases steeply and eventually, at time t_{th}, becomes as large as the loop subchain. After the transition, the decrease of the height of the arm subchain becomes slower, see Fig. 2, reflecting the fact that the number of segments that move with changing brush height becomes larger, see the discussion below eqn (3). Then, towards the end of the loop extrusion process at $t = \tau_{ex}$, the height of the arm subchain decreases steeply to zero. For small α-values it scales approximately as

$$h_{arm}(t) = h_{th} \left(\frac{\tau_{ex} - t}{\tau_{ex} - t_{th}}\right)^\alpha. \qquad (30)$$

The derivation of eqn (30) is shown in S5 in the ESI.‡ The height of the loop subchain increases more steeply than for short time scales, see Fig. 2. The duration of this second time regime, $\tau_{ex} - t_{th}$, decreases with decreasing α. Moreover, for small values of α the increase of the loop height in this regime is small compared to that of the first time regime.

By the time $t = \tau_{ex}$ at which the cohesin reaches the free end, all the segments in the arm subchain have been transferred to the loop region. After the cohesin is unloaded from the free chain end at $t = \tau_{ex}$, the chain relaxes back to its equilibrium state.

The height $h(t)$ of the chain during this relaxation process has the form

$$h(t) = h_{Alx}\left[1 - \left(1 - \frac{h_{ex}^3}{h_{Alx}^3}\right)e^{-3(t - \tau_{ex})/\tau_N}\right]^{1/3}, \qquad (31)$$

where h_{ex} ($= h(\tau_{ex})$) is the height of the chain at $t = \tau_{ex}$. Eqn (31) is derived by using eqn (21).

For the case in which the average loading time τ_{on} is larger than the longest relaxation time τ_N of the chain, the height of the chain returns to its equilibrium value h_{Alx} before a new cohesin is loaded onto the chain. The height h_0 of the chain at the cohesin loading time $t = \tau_{on}$ decreases with decreasing value of τ_{on}, relative to the longest relaxation time τ_N, see Fig. 3. This simply reflects the fact that a new loop extrusion process always starts before the chain had time to relax from the previous extrusion event. For small time scale ratio α, the dependence of the chain height h_0 ($= h(\tau_{on})$) on τ_{on} is approximately given by

$$h_0 = h_{Alx}[1 - (1 - \alpha)e^{-3(\tau_{on}/\tau_N - \alpha)}]^{1/3}, \qquad (32)$$

see the broken curves in Fig. 3. The derivation of eqn (32) is shown in S6 in the ESI.‡ Eqn (32) is derived by using the fact (mentioned earlier) that in the intermediate time regime, $\tau_{th} < t < \tau_{ex}$, the increase of the height of the loop subchain is negligible for small values of α (and thus $h_{ex} \simeq \alpha^{1/3} h_{Alx}$) and by using eqn (31). In the regime of small values of α, the height h_0 decreases with increasing α for fixed (rescaled) average loading time τ_{on}/τ_N, see Fig. 3. On the other hand, the height $h(\tau_{ex})$ at the end of the loop extrusion process shows the opposite dependence on α, see the inset of Fig. 3. In fact, both dependencies reflect the same fact, namely that only the extruded
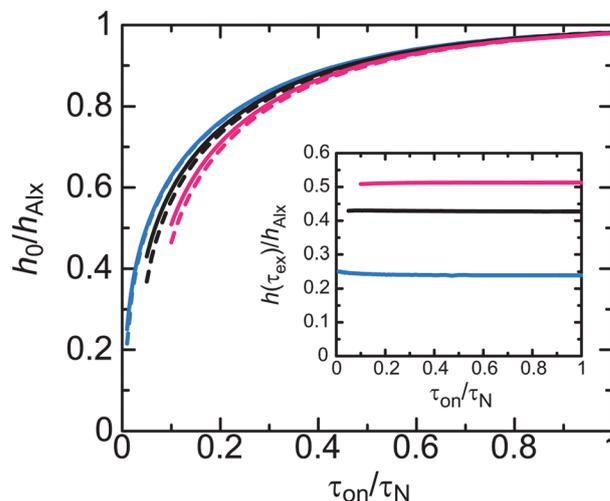

Fig. 3 The chain height h_0 at the time when a cohesin is loaded onto the chain (rescaled by the equilibrium value h_{Alx}, see eqn (23)) is shown as a function of the average loading time τ_{on} (rescaled by the longest chain relaxation time τ_N, see eqn (25)). The values of α used for the calculations are 0.01 (blue), 0.05 (black), and 0.1 (magenta). The solid curves are derived numerically. The broken curves follow from eqn (32). The inset displays the height $h(\tau_{ex})$ (rescaled by h_{Alx}) at the end of the loop extrusion process as a function of the average loading time τ_{on} (rescaled by τ_N) for the same α-values as in the main plot.

subchain can relax during the loop extrusion process, $0 < t < \tau_{ex}$, whereas the rest of the chain has still to pass through the cohesin complex. This means for fast loop extrusion rates (*i.e.* small values of α) that the chain is still rather compact at $t = \tau_{ex}$. At the same time this means that there is now more time available for the relaxation of the whole chain during the time interval $\tau_{ex} < t < \tau_{on}$. However, overall the height h_0 is much more sensitive to the value of τ_{on} than that of τ_{ex}.

The lateral pressure generated by the brush in the steady state has the form

$$\bar{\Pi}_{\parallel} = \frac{1}{\tau_{on}} \int_0^{\tau_{on}} dt \Pi_{\parallel}(t), \qquad (33)$$

where $\Pi_{\parallel}(t) \; (= \Pi_t(t) + \Pi_b(t))$ is the sum of the lateral pressure generated by the chains in the top and bottom layers, see eqn (7) and (8). Our theory predicts that the lateral pressure $\bar{\Pi}_{\parallel}$ increases with decreasing average loading time τ_{on}, see Fig. 4. This is because the loop extrusion process increases the local concentration of chain segments in the vicinity of the interface. In the regime of large average loading time $\tau_{on} > \tau_N$, the lateral pressure has the asymptotic form

$$\bar{\Pi}_{\parallel} = \Pi_{Alx}\left[1 + \frac{\tau_N}{\tau_{on}}\left(\frac{\log 3}{2} - \frac{\pi}{6\sqrt{3}}\right)\right], \qquad (34)$$

for small time scale ratio α, see the black broken curve in Fig. 4. The derivation of eqn (34) is shown in S7 of the ESI.‡ In this regime, chains are in the relaxation process most of the time and thus eqn (34) results from the lateral pressure generated during the relaxation process. In the regime of small average loading time, $\tau_{on} < \tau_N$, the lateral pressure has the approximate form

$$\frac{\bar{\Pi}_{\parallel}}{\Pi_{Alx}} = \frac{1}{3}\frac{\tau_{ex}}{\tau_{on}}\left(3\frac{\tau_{on}}{\tau_N} - \frac{2\tau_{ex}}{\tau_N}\right)^{-1/3} + \frac{1}{2}\frac{\tau_N}{\tau_{on}}\left(3\frac{\tau_{on}}{\tau_N} - \frac{2\tau_{ex}}{\tau_N}\right)^{2/3} \quad (35)$$

for small time scale ratio, see the broken curves in Fig. 4. Eqn (35) is derived by using eqn (27) and by neglecting the lateral pressure generated by the arm subchain in the bottom layer, assuming that $N_b \ll N_{lp}$, see Section S7 of the ESI.‡ This approximation is not effective for moderate values of α, see the black and magenta curves in Fig. 4.

4 Discussion

Our theory predicts that the lateral pressure is mainly generated by the loop extrusion of chains at the interface. This is manifested by the fact the lateral pressure increases as one increases the loading rate τ_{on}^{-1} of cohesins, see Fig. 4. This increase is caused by an increase of the local concentration of chain segments in the vicinity of the interface as a result of loop extrusion.

The lateral pressure opposes the surface tension between the condensate and the nucleoplasm. When the loop extrusion process is suppressed, for example by auxin treatment, Laplace's law predicts that the hydrostatic pressure P_{in} at the interior of the condensate has the form

$$P_{in} - P_0 = \frac{\gamma - \Pi_{Alx}}{r_0}, \qquad (36)$$

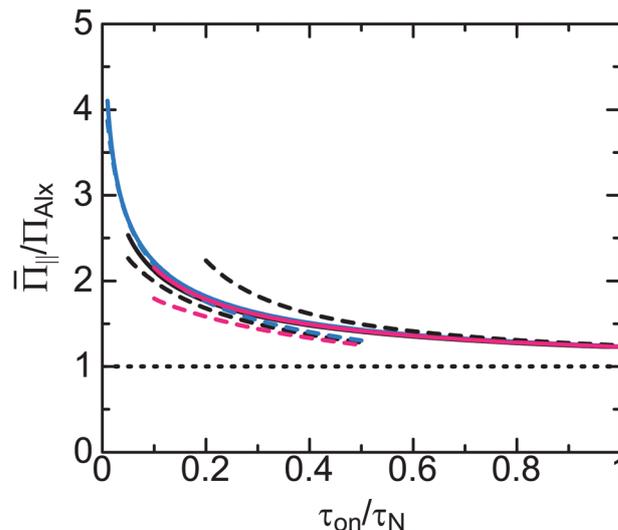**Fig. 4** The lateral pressure $\bar{\Pi}_{\parallel}$ generated by the brush in the steady state (rescaled by the equilibrium value Π_{Alx}) is shown as a function of the average cohesin loading time τ_{on} (rescaled by the longest relaxation time τ_N). The pressure $\bar{\Pi}_{\parallel}$ is defined by eqn (33). For the calculations we chose the following values for α: 0.01 (blue), 0.05 (black), and 0.1 (magenta). The solid curves are derived numerically. The broken curve for large average loading times is given by eqn (34). The broken curves for small loading times correspond to eqn (35).

where γ is the surface tension, P_0 the hydrostatic pressure of the nucleoplasm and r_0 the radius of the condensate. When the loop extrusion process is activated, the hydrostatic pressure P_{in}' at the interior of the condensate now has the form

$$P_{in}' - P_0 = \frac{\gamma - \Pi_{\parallel}}{r_0}. \qquad (37)$$

The fact that the lateral pressure $\Pi_{\parallel}$ generated from the loop extruding brush is larger than the equilibrium pressure Π_{Alx} implies that the hydrostatic pressure at the interior of the condensate decreases by the activation of the loop extrusion process. On a much longer time scale, the molecular components of condensates are transported from condensates of higher hydrostatic pressure to condensates of lower hydrostatic pressure (Ostwald ripening).

The volume of the condensates which colocalize with multiple superenhancers with high cohesin loading rate thus tends to increase. This increases the average distance between the superenhancers (or enhancers separated by a long genomic distance) on the condensate (if the number of superenhancers, or of enhancers at distant genomic distances, on the condensate is constant). This may account for the experimental observation that the contact frequency between superenhancers increases by the auxin treatment.[10] This prediction may be experimentally accessible by measuring the size of condensates and the concentration of the superenhancers that colocalize with the condensates before and after the auxin treatment. Our argument assumes that the condensates in a nucleus are in a transient state and that auxin treatment (or washing auxin out) changes the flux of molecular components. If the condensates are in thermodynamic equilibrium

(or a non-equilibrium steady state), the size of the condensates is determined by the spontaneous curvature. The spontaneous curvature is generated by the distribution of lateral pressure generated by the brush[21] and thus is modulated by the loop extrusion dynamics. Because the loop extrusion increases the concentration of chain segments at the vicinity of the surface, it increases the optimal size of the condensates.

A couple of theories predict the physical mechanism with which the size of protein condensates is tuned. The phase separation of chromatin binding proteins may be driven by a positive feedback: the proteins bound to chromatin induce the condensation of chromatin and, in turn, proteins are attracted to the condensed region.[16,22] Brackley and coworkers used Brownian dynamics simulations and an extension of model B to show that the protein condensates have a stable size when the attractive interactions between the binding proteins and chromatin are switched off at a constant rate because a state transition stops the positive feedback.[23] The state transition may be driven by posttranslational modifications of the binding proteins. Scolari and Lagomarsino treated chromatin as a copolymer in which short blocks that show attractive interactions (mimicking bridging between these blocks by binding proteins) among themselves are incorporated periodically.[24] This theory predicts that chromatin strands are folded into stable micelles, where the attractive short blocks consist of the micelle cores, covered by the corona of the longer blocks. Both of the above mentioned mechanisms predict that chromatin is condensed in the condensates of binding proteins, in contrast to recent experiments that have shown that chromatin tends to be excluded from the condensates of transcription activators and coactivators.[13,14] Therefore these mechanisms might not be relevant to the tuning of the size of the transcription condensates.

At first glance, one might think that the increase of the contact frequency between superenhancers by auxin treatment is explained if the number of superenhancers, which are localized to each condensate, somehow increases. In contrast, our theory predicts that the number of superenhancers in the condensate does not change with the auxin treatment. This prediction is accessible by experiments that measure the concentration of superenhancers in the vicinity of condensates. An alternative explanation may be that auxin treatment somehow drives the coarsening of the condensate. This decreases the total area of the condensate, at which superenhancers are located. The coarsening of condensates produces new interacting partners and it may be detected in Hi-C experiments. In contrast, our theory predicts that the number of superenhancers on a condensate is constant and thus the auxin treatment does not produce new interacting partners. Instead it just increases the contact frequency between already existing interacting partners. The growth mechanism – coarsening vs. Ostwald ripening – can be tested by directly observing the dynamics of condensates. It is thus of interest to characterize the size and number of condensates and the concentration of chromatin in the vicinity of the condensate before and after auxin treatment and to visualize the dynamics of the condensates during the process. Our theory predicts that cohesin is localized at the interface

during the loop extrusion process, which may be detected by measuring the correlation between cohesin and a component of the condensates by using STORM.

In our model, we have used the assumption that the area per chain (or its inverse, the grafting density of the chains) is constant throughout the loop extrusion process. This may correspond to the case in which superenhancers are located at the surface of the condensate relatively densely, when the loop extrusion process is suppressed by the auxin treatment. Our theory treats a relatively short time scale after the loop extrusion is activated at $t = 0$ by washing out auxin, namely the time scale at which the volume of the condensate is still constant. The volume of condensates increases only at a time scale much longer than the time scale of the loop extrusion process. Note that loop extrusion does not operate synchronously on all the chains at the interface. We approximately treat this situation by using the time averaged lateral pressure, see eqn (33). With a more complete treatment, the area per chain at an instance may depend on the dynamics of the neighboring chains and thus may be a function of time. In a mean field picture, the neighboring chains are treated via a constant lateral pressure. The time average of the area per chain is simply the total area at the surface divided by the number of chains on the surface. However, this treatment makes the theory more complex and increases the number of assumptions, such as the treatment of the lateral pressure and area per chain of the two layers. Our theory predicts that the loop extrusion process increases the lateral pressure and this drives the Ostwald ripening that increases the size of the condensate, decreasing the contact frequency between superenhancers. We demonstrate this concept by using a simple model.

We used a couple of assumptions in our theory: (i) we treat cohesin as a motor that extrudes a chromatin fiber with a constant rate (the motor mechanism), as assumed in the loop extrusion theory.[5] However, recent single molecule experiments suggest that cohesin does not act as a molecular motor in vitro.[25–27] Instead the loop extrusion process may be driven by cohesin being pushed by other motors, such as RNA polymerase II.[8] The latter case is not essentially different from the motor mechanism and thus our theory remains applicable. Motivated by an experiment that suggests that cohesin must form dimers to create a chromatin loop,[25] we have theoretically predicted that cohesin dimers extrude chromatin fibers by the osmotic pressure of cohesin monomers.[6] Brackley and coworkers proposed a similar idea, but only with cohesin dimers.[7] Our theory may not be applicable to the osmotic scenario as it is because the chain segments show repulsive interactions and the conformations of the chains at the interface are different from those in the bulk. These may influence the osmotic pressure generated by cohesin monomers. In addition, whether chromatin loops are actually produced by the loop extrusion process is still under debate.[23,24] (ii) We treat chromatin as a brush of flexible polymers. This assumption is motivated by the facts that chromatin tends to be expelled from the transcription condensates,[13,14] it is still associated with the condensates,[11,12] and the transcription activators tend to be associated with the condensates.[11,12] To keep the brush structure, the adhesion between the condensate

and chromatin must be strong enough to counterbalance the tension generated to the chain by the loop extrusion process. The measurement of the magnitudes of the excluded volume interactions between chromatin chain segments will provide quantitative estimate of the lateral pressure generated by the brush.

Our theory treats the chromatin at the surface of a condensate as a loop extruding polymer brush. Although it is a radical simplification, it is tempting to think that the same principle is effective to the original system. The genes that are associated with a condensate are activated by the superenhancers on the condensate, which contains the transcription machinery, such as RNA polymerase II and mediators. The interaction partners of pluripotency genes, such as *Nanog* and *Oct4*, change during differentiation.[28–31] Indeed, with the expression of Yamanaka factors, only the cells that change the interaction partners to those in the pluripotent state are successfully converted to iPS cells.[28] These results imply that the selective association of genes and (super)enhancers is probably the key mechanism of the transcription regulation during differentiation. The growth and regression of transcription condensates are probably the result of the competition between genes for the transcription machinery. The present theory is a step towards the understanding of the physical mechanism of the transcriptional regulation *via* the formation of transcription condensates. It is thus of interest to study the transcription dynamics of genes that are activated by superenhancers on the condensates by using an extension of our present theory.

Conflicts of interest

The authors declare no conflicts of interest.

Acknowledgements

Notes and references

1 J. R. Dixon, S. Selvaraj, F. Yue, A. Kim, Y. Li, Y. Shen, M. Hu, J. S. Liu and B. Ren, *Nature*, 2012, **485**, 376–380.

2 E. P. Nora, B. R. Lajoie, E. G. Schulz, L. Giorgetti, I. Okamoto, N. Servant, T. Piolot, N. L. van Berkum, J. Meisig, J. Sedat, J. Gribnau, E. Barillot, N. Blüthgen, J. Dekker and E. Heard, *Nature*, 2012, **485**, 381–385.

3 S. S. P. Rao, M. H. Huntley, N. C. Durand, E. K. Stamenova, I. D. Bochkov, J. T. Robinson, A. L. Sanborn, I. Machol, A. D. Omer, E. S. Lander and E. L. Aiden, *Cell*, 2014, **159**, 1665–1680.

4 A. L. Sanborn, S. S. P. Rao, S. C. Huang, N. C. Durand, M. H. Huntley, A. I. Jewett, I. D. Bochkov, D. Chinnappan, A. Cutkosky, J. Li, K. P. Geeting, A. Gnirke, A. Melnikov, D. McKenna, E. K. Stamenova, E. S. Lander and E. L. Aiden, *Proc. Natl. Acad. Sci. U. S. A.*, 2015, **112**, E6456–E6465.

5 G. Fudenberg, M. Imakaev, C. Lu, A. Goloborodko, N. Abdennur and L. A. Mirny, *Cell Rep.*, 2016, **15**, 2038–2049.

6 T. Yamamoto and H. Schiessel, *Phys. Rev. E*, 2017, **96**, 030402(R).

7 C. A. Brackley, J. Johnson, D. Michieletto, A. N. Morozov, M. Nicodemi, P. R. Cook and D. Marenduzzo, *Phys. Rev. Lett.*, 2017, **119**, 138101.

8 B. A. Busslinger, R. R. Stocsits, P. van der Lelij, E. Axelsson, A. Tedeschi, N. Galjart and J. M. Peters, *Nature*, 2017, **544**, 503–507.

9 T. Natsume, T. Kiyomitsu and Y. S. M. Kanemaki, *Cell Rep.*, 2016, **15**, 210–218.

10 S. S. P. Rao, S. C. Huang, B. G. S. Hilaire, J. M. Engreitz, E. M. Perez, K. R. Kieffer-Kwon, A. L. Sanborn, S. E. Johnstone, G. D. Bascom, I. D. Bochkov, X. Huang, M. S. Shamim, J. Shin, D. Turner, Z. Ye, A. D. Omer, J. T. Robinson, T. Schlick, B. E. Bernstein, R. Casellas, E. S. Lander and E. L. Aiden, *Cell*, 2017, **171**, 305–320.

11 B. R. Sabari, A. Dall'Agnese, A. Boija, I. A. Klein, E. L. Coffey, K. Shrinivas, B. J. Abraham, N. M. Hannett, A. V. Zamudio, J. C. Manteiga, C. H. Li, Y. E. Guo, D. S. Day, J. Schuijers, E. Vasile, S. Malik, D. Hnisz, T. I. Lee, I. I. Cisse, R. G. Roeder, P. A. Sharp, A. K. Chakraborty and R. A. Young, *Science*, 2018, **361**, eaar3958.

12 A. Boija, I. A. Klein, B. R. Sabari, A. Dall'Agnese, E. L. Coffey, A. V. Zamudio, C. H. Li, K. Shrinivas, J. C. Manteiga, N. M. Hannett, B. J. Abraham, L. K. Afeyan, Y. E. Guo, J. K. Rimel, C. B. Fant, J. Schuijers, T. I. Lee, D. J. Taatjes and R. A. Young, *Cell*, 2018, **175**, 1842–1855.

13 Y. Shin, Y. Chang, D. Lee, J. Berry, D. Sanders, P. Ronceray, N. Wingreen, M. Haataja and C. Brangwynne, *Cell*, 2018, **175**, 1481–1491.

14 L. Hilbert, Y. Sato, H. Kimura, F. Jülicher, A. Honigmann, V. Zaburdaev and N. L. Vastenhouw, *BioRxiv*, 2018.

15 T. Yamamoto, T. Sakaue and H. Schiessel, *Europhys. Lett.*, 2019, submitted.

16 T. Yamamoto and H. Schiessel, *Langmuir*, 2016, **32**, 3036–3044.

17 T. Yamamoto and H. Schiessel, *Soft Matter*, 2017, **13**, 5307–5316.

18 S. Alexander, *J. Phys.*, 1977, **38**, 983–987.

19 P. de Gennes, *Macromolecules*, 1980, **13**, 1069–1075.

20 M. Doi, *Soft Matter Physics*, Oxford University Press, Oxford, UK, 2013.

21 S. Safran, *Statistical Thermodynamics of Surfaces, Interfaces, and Membranes*, Westview Press, CO, USA, 2003.

22 C. Brackley, S. Taylor, A. Papantonis, P. Cook and D. Marenduzzo, *Proc. Natl. Acad. Sci. U. S. A.*, 2013, **110**, E3605–E3611.

23 C. Brackley, B. Liebchen, D. Michieletto, F. Mouvet, P. Cook and D. Marenduzzo, *Biophys. J.*, 2017, **112**, 1085–1093.

24 V. Scolari and M. Lagomarsino, *Soft Matter*, 2015, **11**, 1677–1687.

25 J. Stigler, G. Camdere, D. Koshland and E. Greene, *Cell Rep.*, 2016, **15**, 988–998.

26 I. Davidson, D. Goetz, M. Zaczek, M. Molodtsov, P. H. I. Veld, F. Weissmann, G. Litos, D. Cisneros, M. Ocampo-Hafalla, R. Ladurner, F. Uhlmann, A. Vaziri and J. Peters, *EMBO J.*, 2016, **35**, 2671–2685.

27 M. Kanke, E. Tahara, P. H. I. Veld and T. Nishiyama, *EMBO J.*, 2016, **35**, 2686–2698.

28 H. Zhang, W. Jiao, L. Sun, J. Fan, M. Chen, H. Wang, X. Xu, A. Shen, T. Li, B. Niu, S. Ge, W. Li, J. Cui, G. Wang, J. Sun, X. Fan, X. Hu, R. Mrsny, A. Hoffman and J. F. Hu, *Cell Stem Cell*, 2013, **13**, 30–35.

29 J. Phillips-Cremins, M. Sauria, A. Sanyal, T. Gerasimova, B. Lajoie, J. Bell, C. Ong, T. Hookway, C. Guo, Y. Sun, M. Bland, W. Wagstaff, S. Dalton, T. McDevitt, R. Sen, J. Dekker, J. Taylor and V. Corces, *Cell*, 2013, **153**, 1281–1295.

30 Z. Wei, F. Gao, S. Kim, H. Yang, J. Lyu, W. An, K. Wang and W. Lu, *Cell Stem Cell*, 2013, **13**, 36–47.

31 E. Apostolou, F. Ferrari, R. Walsh, O. Bar-Nur, M. Stadtfeld, S. Cheloufi, H. Stuart, J. Polo, T. Ohsumi, M. Borowsky, P. Kharchenko, P. Park and K. Hochedlinger, *Cell Stem Cell*, 2013, **12**, 699–712.